

Phase transition between two different orientations of the Q phase in the NaNbO_3 thin film

A. V. Pavlenko,^{1,2} D. V. Stryukov,² M. V. Vladimirov,³ A. E. Ganzha,³ S. A. Udovenko,³ Anjana Joseph,⁴ Janaky Sunil,⁴ Chandrabhas Narayana,⁴ R. G. Burkovsky,³ I. P. Raevski,¹ and N. V. Ter-Oganessian^{1,*}

¹*Institute of Physics, Southern Federal University, 344090 Rostov-on-Don, Russia*

²*Southern Scientific Center, Russian Academy of Sciences, 344006 Rostov-on-Don, Russia*

³*Peter the Great Saint-Petersburg Polytechnic University, 195251 St. Petersburg, Russia*

⁴*Jawaharlal Nehru Centre for Advanced Scientific Research, 560064 Bangalore, India*

(Dated: December 10, 2021)

Temperature evolution of dielectric response, atomic structure, and lattice dynamics in thin film of sodium niobate in the epitaxial $\text{NaNbO}_3/\text{SrRuO}_3/(001)\text{MgO}$ heterostructure is studied by dielectric measurements, x-ray diffraction, and Raman spectroscopy. It is found that at room temperature NaNbO_3 is in ferroelectric state, whereas the temperature-dependent dielectric constant experiences a broad maximum at 440 K on cooling and at 500 K on heating and reveals a diffuse phase transition. Reciprocal space mapping shows the presence of both anti-phase and in-phase tilting of oxygen octahedra. The temperature dependence of the M-point reflections suggests reorientation of the in-phase octahedra tilting axis from being parallel to the substrate at room temperature to perpendicular orientation at high temperatures. The temperature evolution of the shape of the Raman spectra reveal the decrease of the number of constituting peaks on heating. These results are interpreted as indicating a temperature-driven transition between two different orientations of the bulk ferroelectric Q phase with respect to the interface, namely between the state with electric polarization pointing at $\approx 45^\circ$ to the normal at room temperature to the state with polarization parallel to the interface above the transition. Transitions of this kind can be anticipated from theoretical considerations, while the experimental evidences of such are yet scarce.

I. INTRODUCTION

Sodium niobate, NaNbO_3 (NNO), has been studied since several decades. Because of the presence of at least six temperature-induced phase transitions at ambient pressure, NaNbO_3 is known as arguably the most complex perovskite, which makes this compound methodologically interesting [1, 2]. Sodium niobate has ferroelectric ground state and room temperature antiferroelectric (AFE) phase, which, combined with its lead-free composition, makes it also promising for energy storage, electrocaloric, electromechanical, and other applications [3–8].

Seven phases are commonly assumed in NaNbO_3 with more or less well-established crystal symmetry, however subtle differences between some phases still lead to debates in literature [9–11]. The low-temperature rhombohedral ferroelectric phase N, that is stable below 173 K, has space group $R3c$. Above this temperature centrosymmetric phases are stable: P (sp. gr. $Pbcm$, 173 K – 633 K), R (sp. gr. $Pmmn$, 633 K – 753 K), S (sp. gr. $Pmmn$, 753 K – 793 K), T_1 (sp. gr. $Ccmm$, 793 K – 848 K), T_2 (sp. gr. $P4/mbm$, 848 K – 913 K), and U (sp. gr. $Pm\bar{3}m$, above 913 K). These phase transition temperatures naturally vary slightly from one work to another, except for the N – P phase transition temperature, which strongly depends on the quality of the crystal, the presence of defects and impurities [12]. Some authors also

conclude on the coexistence of phases, e.g., the coexistence of the N and P phases over a wide temperature range between 12 and 280 K [9, 13].

In some studies of bulk NaNbO_3 , in the temperature region of the P phase, ferroelectric Q phase with $P2_1ma$ symmetry is observed instead [14]. This phase can appear in NaNbO_3 samples with defects or slight variations in composition, but is also induced by application of electric field, which confirms the AFE nature of the P phase [15–17]. The Q phase was also reported in NaNbO_3 powders with particle sizes below 400 nm and ceramics with fine grains [18–20]. It has to be noted, that reversible P – Q electric field-induced transition was only observed in high quality single crystals [21–23], which means that in nominally pure NaNbO_3 after removal of electric field the Q phase does not revert back to the P phase but is believed to be pinned by defects or due to rather high potential barrier between the two phases. This also evidences that both phases have similar thermodynamic potential values and that of the P phase is slightly more preferable.

Based on the aforementioned facts, it is commonly believed that several structural instabilities resulting in the variety of crystal structures come into play in sodium niobate and the fragile balance between them determines the complex sequence of the observed phase transitions. Therefore, the analysis of the principal distortion modes that result in the observed phases is crucial for the proper understanding of the phase transition sequence. Such structural mode analysis of NaNbO_3 was first performed by Cochran and Zia [24] and recently extended by Tolédano and Khalyavin [25]. The authors conclude that the driving modes belong to several points in the

* teroganessian@sfned.ru

Brillouin zone including Γ , R, M, and T. These modes, which appear in different combinations in different phases of NaNbO_3 , have the largest amplitudes and determine their symmetry, whereas other modes are induced in improper way.

Thin films of sodium niobate attract interest of researchers because of possibility of tailoring its properties for technological applications [26–28]. Owing to the mechanical constraints imposed by the substrate, size effects, the appearance of dead layers, etc., thin films of NaNbO_3 may show physical properties and phase transitions sequences that substantially differ from those of the bulk due to the different influences of these factors on the aforementioned modes.

Thin films of NaNbO_3 have been fabricated by different methods including pulsed laser [29–33] and metal organic chemical vapor deposition [34–36], magnetron [37] and radio-frequency cathode sputtering [38]. To characterize the structure and properties of the films, x-ray $\theta/2\theta$ diffraction and reciprocal space mapping [34–37], transmission electron microscopy [30, 31], Raman spectroscopy [29], temperature-dependent dielectric studies [30, 33, 34], electric polarization loops measurement [31, 32, 37], and piezoelectric force microscopy [30, 31, 35, 36] methods are commonly employed. With the help of the aforementioned techniques the following results, that are pertinent to the present study, were obtained.

$\text{NaNbO}_3/\text{SrRuO}_3/\text{SrTiO}_3$ films with differently oriented substrates [(001), (110), and (111)] showed ferroelectric P - E polarization loops with the largest polarization in the (110) oriented film [32]. A fourfold multiplication of the unit cell perpendicular to the (001) SrTiO_3 substrate was found by Yamazoe *et al.* [30], which allowed the authors to conclude on the $Pbma$ symmetry of the film that was supported by the antiferroelectric-like dielectric anomaly at 645 K. The films with (110) and (111) orientations of SrTiO_3 showed a broad dielectric anomaly around 673 K and a twofold multiplication of the unit cell, which let the authors claim the film to have the $P2_1ma$ symmetry (Q phase) [30]. Sodium niobate films were also deposited on several other perovskite-like (110)-oriented orthorhombic substrates, e.g., NdGaO_3 , TbScO_3 , DyScO_3 , GdScO_3 [34–36]. Deposited on such substrates, NaNbO_3 exhibits slightly different in-plane lattice parameters a and b , which results in in-plane anisotropic dielectric properties, whereas the crystal symmetry was found to be $Pmc2_1$ ($= P2_1ma$, Q phase) in some works [34, 36].

Several works reported on the synthesis of NaNbO_3 films on MgO , which is another frequently used substrate. The type of the substrate can substantially influence the properties of the film despite the same intermediate layer. Thus, $\text{NaNbO}_3/\text{SrRuO}_3$ grown on (001) SrTiO_3 or (001) MgO can in principle show different properties. $\text{NaNbO}_3/\text{SrRuO}_3/(001)\text{MgO}$ films with K-Ta-O or Pt buffers obtained by pulsed laser deposition and RF magnetron sputtering, respectively, were reported to show

different pseudotetragonal unit cell parameters [31, 37]. The former film showed superstructure along the c -axis direction with fourfold multiplication of the lattice constant and both films were found to be ferroelectric with remanent polarizations of 6.4 and 20 $\mu\text{C}/\text{cm}^2$, respectively. Using micro-Raman spectroscopy Yuzyuk *et al.* reported on the Q phase stability up to ~ 600 K in a 250 nm thick $\text{NaNbO}_3/(\text{La}_{0.5}\text{Sr}_{0.5})\text{CoO}_3/(001)\text{MgO}$ film [29], whereas Tyunina and Levoska also reported a dielectric anomaly around 330 $^\circ\text{C}$ [33].

Thin films of NaNbO_3 were studied theoretically by Diéguez *et al.* [39] using density functional theory (DFT) calculations, who determined the direction of electric polarization depending on misfit strain. This approach, which follows the original works of Pertsev *et al.* [40–42] allows calculating phase diagrams in temperature-epitaxial strain coordinates. These diagrams can generally contain phases with the same symmetry that differ only in orientation of the electric polarization. In case of an unstrained bulk crystal these phase states can actually become different domains of the same phase. However, in the case of epitaxial conjugation of the film with the substrate resulting in misfit strain, they can become different phases, resulting in a possibility of phase transition between them with respective anomalies in dielectric constant as, for example, predicted for the phase transition in PbTiO_3 between the c -phase and the polydomain $a_1/a_2/a_1/a_2$ state [42].

The phase transitions in NNO are due to interplay of several instabilities, which requires taking into account several order parameters that are not considered in the aforementioned approach. Recently, Patel *et al.* [43] also considered the effect of epitaxial strain on (001) NaNbO_3 films using DFT method and obtained a phase diagram by comparing the energies of different structures of NNO. The diagram was found to include the monoclinically distorted N phase, the Q phase, and the polar phase stemming from the bulk P structure, in which electric polarization additionally appears, thus, lowering the symmetry from $Pbcm$ to $Pca2_1$. It has to be noted, though, that thorough comparison of theoretical results with experimental findings is still lacking, which is to some extent limited by the frequent absence of reports of the experimentally observed lattice parameters or difficulties in determination of the appearing crystal structure.

Summarizing the main results on the temperature-dependent structural and dielectric properties of NNO films, one can note the appearance of ferroelectric phases at room temperature, observation of two- or fourfold unit cell multiplication in one of the crystal axis directions, occurrence of a maximum in the temperature-dependent dielectric constant. It has to be noted, though, that usually the crystal symmetry of the NNO film, i.e., the Q or the P phase, is established only upon the presence of two- or fourfold multiplication of the pseudocubic unit cell. Since the NNO films with fourfold multiplication in some cases show electric polarization, it remains unclear, for example, whether its structure is related to the

mentioned $Pca2_1$ phase [43]. Another important open question is: What is the origin of the temperature-induced phase transition manifested in the maximum of the temperature-dependent dielectric constant and how it is related to the dielectric constant maximum at the P-R transition in the bulk? To the best of our knowledge, these questions have not been addressed by any structural temperature-dependent studies, which could shed light on the relation between the crystal structures and phase transition sequence in the film and the bulk forms of NaNbO_3 .

Motivated by these problems, in this work we study the phase transition in sodium niobate in the $\text{NaNbO}_3/\text{SrRuO}_3/(001)\text{MgO}$ heterostructure. Using complementary methods including temperature-dependent dielectric, structural, and Raman spectroscopy studies we find a broad phase transition above room temperature. This phase transition is manifested in a broad maximum of the dielectric constant, reorientation of the octahedra tilting axes, and the change in the number of observed Raman modes. The results suggest that this transition is a phase transition between two different orientations of the bulk Q phase with differently oriented polarizations. Similar phase transitions have been actively studied earlier theoretically using phenomenological models [40–42, 44]. In particular, strain-induced transitions were predicted in PbTiO_3 and BaTiO_3 between states with different orientations of electric polarization, which formally have the same symmetry but should be treated as different phases. The experimental evidence of such temperature-induced phase transitions, which we observe in our work, is still limited.

II. EXPERIMENTAL

The films of NaNbO_3 and SrRuO_3 , which was used as the bottom electrode, in the $\text{NaNbO}_3/\text{SrRuO}_3/(001)\text{MgO}$ [$\text{NNO/SRO}/(001)\text{MgO}$] heterostructure were prepared by RF sputtering method using the "Plasma 50 SE" apparatus. Single-crystalline $\text{MgO}(001)$ with thickness of 0.5 mm (MTI Corp.) was employed as substrate. The temperature of the substrates in the chamber before switching on the RF discharge was 673 K and 783 K after switching on, the RF power was 120 W, whereas the distance between the target and the furnace with the substrate was 15 mm. First, SrRuO_3 was sputtered on MgO to obtain $\text{SrRuO}_3/(001)\text{MgO}$, which was followed by NaNbO_3 sputtering resulting in the sought heterostructure. For the dielectric and Raman spectroscopy measurements the thicknesses of the NNO and SRO films were 750 and 150 nm, respectively, which was suitable for dielectric studies and ensured proper shielding of MgO substrate in Raman measurements, whereas for the x-ray diffraction measurements the thicknesses were 150 and 20 nm, respectively, which ensured the absence of noticeable reflections of SRO in reciprocal space mapping.

To conduct dielectric measurements in the direction perpendicular to the film plane, electrodes were deposited on the free surface of the film by thermal evaporation of Al in vacuum through a mask with holes with a diameter of 180–200 μm , whereas SrRuO_3 acted as the lower electrode. The area of electrodes was measured using the Keyence VK-9700 3D microscope (Joint Center for Scientific and Technological Equipment, Scientific Center of the Russian Academy of Sciences). The temperature dependences of the dielectric constant at frequencies of 10^4 and 10^5 Hz with an amplitude of 0.04 V were obtained using an LCR 4263B meter (Agilent Technologies). The capacitance-voltage $C(U)$ and $P(E)$ dependencies were measured using a TF Analyzer 2000 (Center for Collective Usage of the Institute of Physics, Southern Federal University, Rostov-on-Don, Russia).

X-Ray diffraction (XRD) measurements were carried out on SuperNova (Rigaku) X-Ray diffractometer (Research and Education center "Physics of Nanocomposite Materials", Peter the Great St. Petersburg Polytechnic University). To characterize sodium niobate film in the NNO/SRO/MgO heterostructure single crystal diffraction method with grazing incidence geometry was used. The incident radiation ($\text{Cu K}\alpha$) was scattered on the heterostructure, and the scattered radiation was registered on the detector (Atlas CCD Detector, Agilent Technologies). Two diffraction experiments were performed. In the first experiment ω , θ , and κ angles were 72° , 60° , and -134° , respectively, while ϕ was changing from 0° to 180° with a step of 0.25 (1.00) $^\circ$. Detector distance was 50 mm and exposure time was 10 (6) seconds. In the second experiment ω , θ , and κ angles were 70° , 70° , and -105° , respectively, while ϕ was changing from -70° to 200° with a step of 1° . Detector distance was 50 mm and exposure time was 10 seconds. The frames obtained from the experiments were used to construct reciprocal space maps.

Raman spectroscopic measurements were conducted using LabRam HR Evolution micro-Raman spectrometer, which has an assembly of 532 nm Nd:YAG solid state four level laser, an 800 mm focal length monochromator and a Peltier-cooled CCD detector (Jawaharlal Nehru Centre for Advanced Scientific Research, Bangalore, India). Each spectrum was collected in 180° backscattering geometry using a 50x objective, with an average acquisition time of 1 minute and an incident power of ~ 20 mW. The LabSpec6 software recorded the spectra in spectral range $100 - 1000 \text{ cm}^{-1}$, with the spectral resolution of around 1 cm^{-1} for the grating of 1800 grooves per mm^{-1} . The temperature-dependent Raman studies were done from 298 K to 850 K, employing the Linkam THMS 600 cryostage with a temperature controller (Linkam TMS 94), which maintains the set temperature with an accuracy of ± 0.1 K.

TABLE I. Ferroelectric $P(E)$ loop parameters for the 340 kV/cm electric field amplitude

Parameter	Value
E_{c+} , kV/cm	111.6
E_{c-} , kV/cm	-78.04
P_{r+} , $\mu\text{C}/\text{cm}^2$	11.4
P_{r-} , $\mu\text{C}/\text{cm}^2$	-16.4
P_{rrel+} , $\mu\text{C}/\text{cm}^2$	11.21
P_{rrel-} , $\mu\text{C}/\text{cm}^2$	-15.9
P_{max+} , $\mu\text{C}/\text{cm}^2$	24.3
P_{max-} , $\mu\text{C}/\text{cm}^2$	-24.3
W_{loss} , $\mu\text{J}/\text{cm}^2$	809

III. RESULTS

A. Dielectric studies

Our electric measurements indicate the presence of a ferroelectric phase at room temperature and a transition upon heating, as evidenced from ferroelectric hysteresis loops and the maximum in the temperature dependence of the dielectric constant. Figures 1(a)-(d) show dielectric constant dependencies of the Al/NNO/SRO/(001)MgO heterostructure on applied electric field $\varepsilon(E)$ measured at various frequencies f_{ext} of external triangular signal. At room temperature the NaNbO₃ film has a dielectric constant of $\varepsilon \sim 900$ and a rather low loss tangent $\tan \delta \sim 0.02 - 0.11$. Independent of f_{ext} the $\varepsilon(E)$ dependencies have a butterfly form characteristic of ferroelectric structures, possess hysteresis, and have high dielectric tunability [$\varepsilon(E = 0 \text{ kV/cm}) - \varepsilon(E = 100 \text{ kV/cm})$]/ $\varepsilon(E = 0 \text{ kV/cm}) \approx 0.5$.

Figures 1(e) and (f) show electric polarization and electric current at different amplitudes of applied electric field. The dependencies possess characteristic ferroelectric form, which suggests that the NaNbO₃ film at room temperature in the studied heterostructure is in the ferroelectric state. Table I provides the main ferroelectric properties of the NNO film calculated from the $P(E)$ loop for the electric field amplitude of 340 kV/cm. The asymmetric form of the $P(E)$ loops reveals itself in the differences of coercive fields and remanent polarizations, which suggests the presence of internal field in the NNO film.

The temperature dependence of the dielectric constant shown in Fig. 1(g) reveals a broad maximum, whose position is independent on frequency. On heating, the dielectric maximum occurs at $T_m = 500 \text{ K}$, whereas on cooling at $T_m = 440 \text{ K}$. Thus, according to the temperature dependence of the dielectric constant, the NaNbO₃ film experiences a phase transition in the temperature range 440 – 500 K characterized by large thermal hysteresis. In order to shed light on the origin of this phase transition we performed temperature-dependent x-ray reciprocal space mapping and Raman spectroscopy studies, the results of which are described in the following sections.

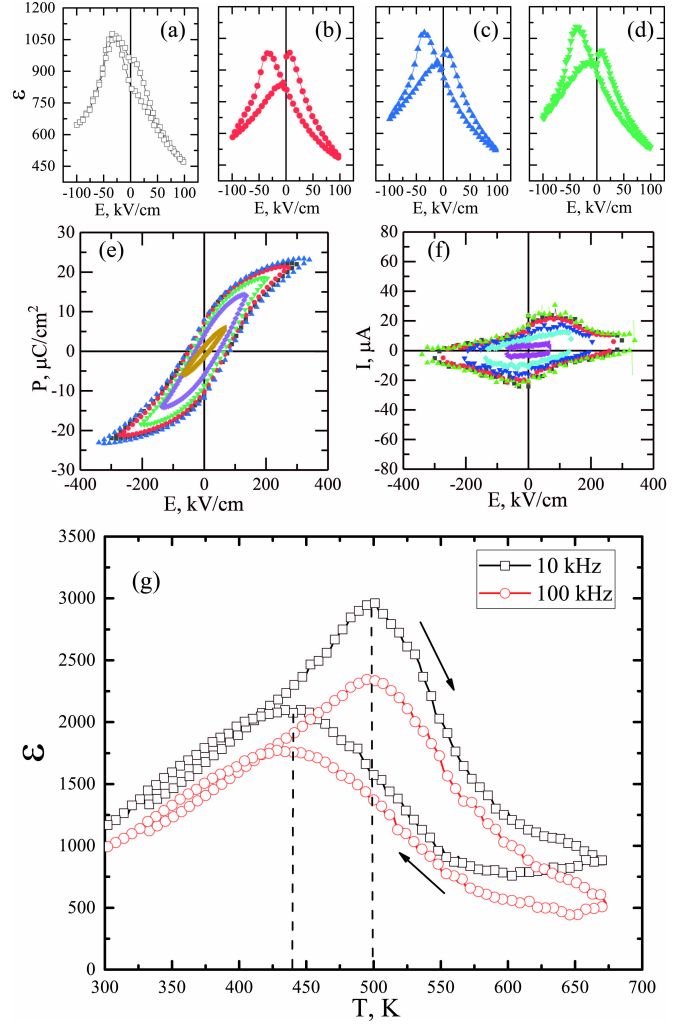


FIG. 1. (a) – (d) Dielectric constant dependencies on electric field $\varepsilon(E)$. The frequency of the measurement electric field with the amplitude 40 mV is 100 kHz and the cycle frequencies are: (a) – $f_{\text{ext}} = 1 \text{ Hz}$, (b) – $f_{\text{ext}} = 5 \text{ Hz}$, (c) – $f_{\text{ext}} = 10 \text{ Hz}$, (d) – $f_{\text{ext}} = 40 \text{ Hz}$. Electric polarization $P(E)$ (e) and electric current $I(E)$ (f) as functions of applied electric field at room temperature and the frequency of 1 kHz. (g) Temperature dependence of the dielectric constant of Al/NNO/SRO/(001)MgO heterostructure.

B. Reciprocal space imaging

1. Room temperature

To study the crystal structure of sodium niobate we performed x-ray reciprocal space mapping. Three sets of reflections can be expected in diffraction from the NNO/SRO/MgO heterostructure, i.e., one from the substrate and two from the NNO and SRO films, however only those from NNO and MgO are observed due to the small thickness of the intermediate layer SrRuO₃. The pseudocubic reciprocal space grid is based on the so-called main reflections from NNO, which is the object

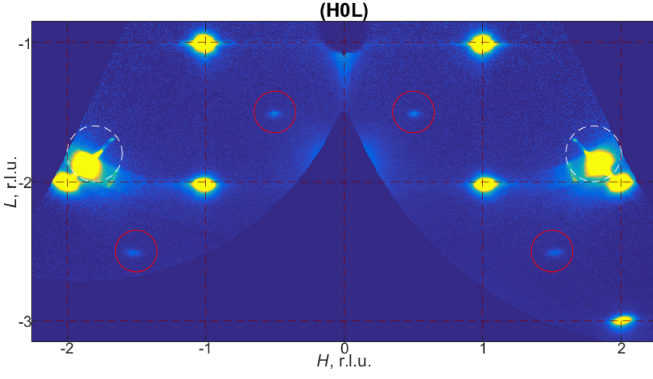


FIG. 2. (H0L) plane of reciprocal space for the NNO/SRO/MgO heterostructure at room temperature. Intensity peaks at $(H + \frac{1}{2}, 0, L + \frac{1}{2})$ are superstructural reflections from NNO (marked by red circles). Intensity peaks at $\approx (\pm 1.8, 0, -1.8)$ are MgO reflections (marked by white circles).

of the study (Fig. 2).

In addition to reflections in Γ (HKL) positions of the pseudocubic Brillouin zone (PCBZ), superstructural reflections in R- and M-points are found, which are shown in Fig. 3(a). The family of M-points consists of reflections in $M_H = (H, K + \frac{1}{2}, L + \frac{1}{2})$, $M_K = (H + \frac{1}{2}, K, L + \frac{1}{2})$, and $M_L = (H + \frac{1}{2}, K + \frac{1}{2}, L)$ positions. At room temperature the reflections in M_L points are very weak, as can be seen in Fig. 3(b).

The set of observed superstructural reflections, taking into account their presence or absence in certain places of the reciprocal space, makes it possible to characterize the distorted structure. The first point to note is that M point reflections are observed only in points with symmetric coordinates, i.e., when the two half-integer coordinates are equal in magnitude. Such a condition for systematic absence of reflections exists only for two distortion modes in M point, namely, for the case of M^{2+} (in-phase tilting of octahedra) and M^{3+} (distortions of octahedra). Here and in the following we assume that Na is in the origin of the pseudocubic unit cell. Assuming that distortions are unlikely, because they are energetically less favorable, one can conclude that the M point reflections are due to in-phase tilting of octahedra. Similarly, since no reflections are observed at symmetric (all coordinates equal in magnitude) R points, which is only compatible with the R^{5-} mode, the corresponding structural changes are due to anti-phase tilting of octahedra. Therefore, from reciprocal space mapping one can conclude that both in-phase and anti-phase tilting of octahedra are observed in the film at room temperature. This is compatible with the ferroelectric Q phase as shown in Figs. 4(a) and (b).

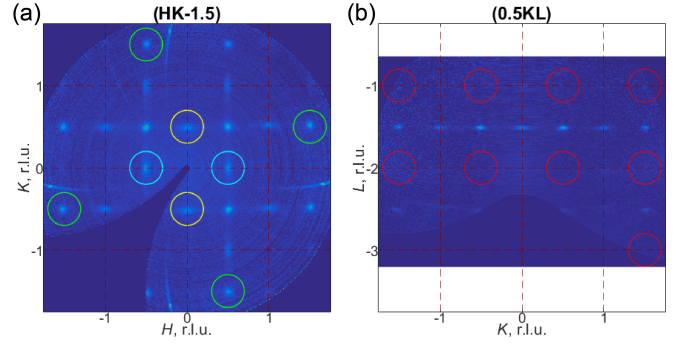


FIG. 3. Room temperature reciprocal space maps of the NNO/SRO/MgO heterostructure. (a) ($HK - 1.5$) plane: superstructural reflections at M_H , M_K , and R positions of the PCBZ are marked by yellow, cyan, and green circles, respectively. (b) ($0.5KL$) plane: almost vanishing superstructural reflections at M_L positions marked by red circles can be seen.

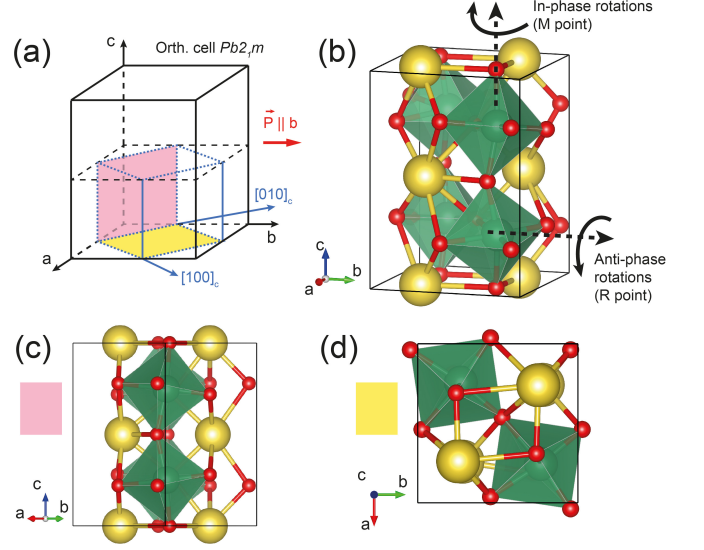


FIG. 4. (a) The orthorhombic unit cell of the Q phase (black) and the constrained pseudocubic faces (shaded yellow and pink). The pseudocubic cell is shown in blue. Red arrow gives the direction of electric polarization. (b) Orthorhombic unit cell of the Q phase. The dark yellow and red spheres represent Na and O atoms, respectively, whereas NbO_6 octahedra are shown in green. (c) Top view of the "pink"-type epitaxy. (d) Top view of the "yellow"-type epitaxy.

2. Temperature-dependent studies

In order to study the evolution of the structure with temperature we performed reciprocal space mapping in the temperature range 298 – 773 K. Upon heating, starting from room temperature a gradual extinction of superstructural reflections in M_H and M_K points occurs as shown in Fig. 5(a). These reflections do not disappear completely in the studied temperature range, as can be seen in Fig. 5(d,e). The same holds for the intensities in the R-point however to a lower extent, as shown in

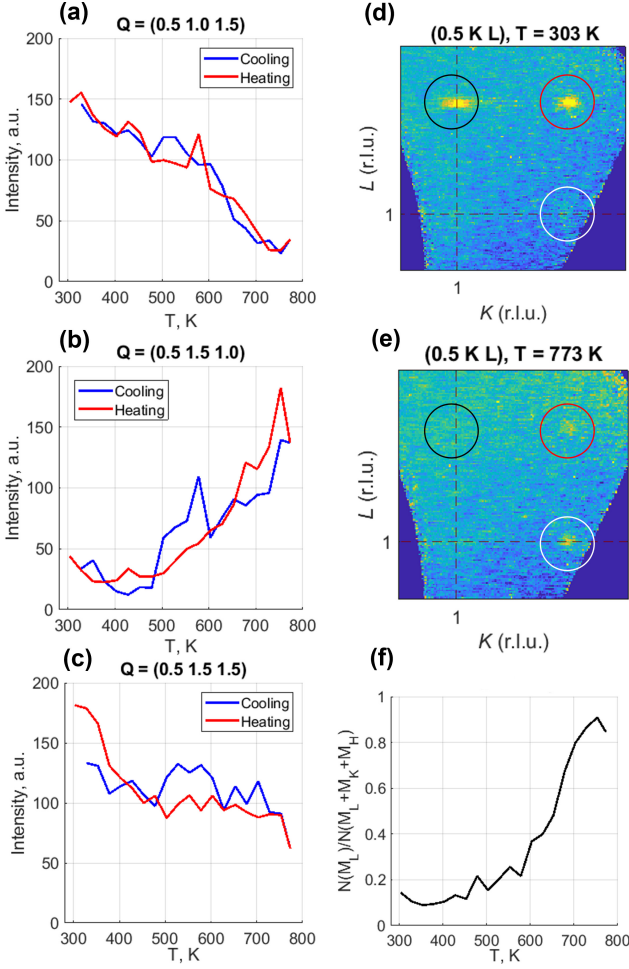


FIG. 5. Intensities of superstructural reflections at the M_K ($\frac{1}{2}, 1, \frac{3}{2}$) point corresponding to in-phase rotations of octahedra around the axis parallel to the substrate (a), at the M_L ($\frac{1}{2}, \frac{3}{2}, 1$) point corresponding to the in-phase rotations of octahedra around the axis normal to the substrate (b), and at the R ($\frac{1}{2}, \frac{3}{2}, \frac{3}{2}$) point corresponding to anti-phase rotations (c). (d-e) ($\frac{1}{2}KL$) planes at different T (M_K , M_L , and R points are marked by black, white, and red circles, respectively). (f) Volume fraction of domains with reflections in the M_L -points.

Fig. 5(c). On the other hand, with heating the intensities at the M_L -points increase as shown in Fig. 5(b). The results of the temperature-dependent studies indicate occurrence of a diffuse phase transition between two different structures, which starts at room temperature and extends at least to the highest measured temperature (773 K). This phase transition can be interpreted as between two different orientations of the Q phase, which we denote by "pink" and "yellow" shaded faces in Fig. 4(a) that have to be constrained to the underlying substrate as shown in Figs. 4(c) and (d). The details of these structures will be discussed below. Based on the intensities of reflections in M_H , M_K , and M_L points one can calculate the temperature evolution of the relative ratio of different phases, which is shown in Fig. 5(f).

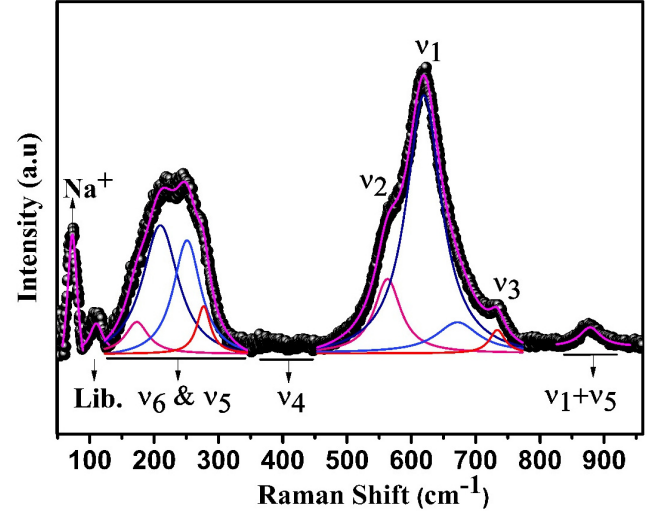


FIG. 6. Raman spectrum of NNO/SRO/MgO thin film at room temperature with mode assignment showing the translational mode of Na^+ , the librational mode, and the modes $\nu_1 - \nu_6$ that stem from vibrations of a NbO_6 octahedron with O_h symmetry.

C. Raman spectroscopy

To further understand how the structure changes with the temperature, we have carried out temperature-dependent Raman Spectroscopy on the NNO/SRO/MgO heterostructure from 298 to 853 K. The Raman spectrum recorded at ambient conditions is shown in Fig. 6 and the modes are assigned as the translational modes of Na^+ cation, librational modes, and internal vibrations of NbO_6 octahedra ($\nu_1 - \nu_6$) based on the earlier reported studies on $NaNbO_3$ powder, single crystals, and ceramics [18, 45–52]. Here the modes $\nu_1 - \nu_6$ stem from those of an ideal undistorted NbO_6 octahedron with O_h symmetry [53]. The spectra at room temperature mainly consist of two broad asymmetric bands, and both were fitted into four Lorentz peaks each. As shown in Fig. 6, the ν_1 , ν_2 , and ν_3 phonon modes of NbO_6 octahedral vibrations were seen together as the most intense band around 450–780 cm^{-1} and the ν_5 and ν_6 bands were found to be converged as a broad, second most intense band ranging from 130 to 340 cm^{-1} . The ν_4 modes were observed to be very weak and the weak band at 877 cm^{-1} is assigned to the $\nu_1 + \nu_5$ combination mode. In addition, there are two relatively sharp peaks observed around 73 cm^{-1} and 110 cm^{-1} , which are assigned to the external vibration related to the translational movements of Na^+ cations and the librations of the NbO_6 octahedra, respectively [18, 45–52]. As compared to the Raman spectra of bulk $NaNbO_3$ in P phase, remarkable differences were observed in our thin film spectra such as the reduced number of modes (especially the external vibrations of Na^+ cations and librational modes of NbO_6 octahedra) and the increased broadness of the internal octahedral

vibrations [18, 29, 45–52]. Similar observations in Raman spectra were also seen in the Q phase reported in NaNbO_3 powders with particle sizes below 400 nm [18]. As compared to the NNO single crystal, the absence of modes around 96 and 154 cm^{-1} , the overlapping modes in the broad bands and the shifting of modes from 557 and 601 cm^{-1} to 564 and 620 cm^{-1} , respectively, suggest that the phase occurring in the NNO thin film is the ferroelectric Q phase, similar to that of the earlier reported ceramic and thin film samples [29, 51]. This conclusion is correlating well with our results from X-ray reciprocal space imaging too.

The temperature evolution of Raman spectra of NNO thin film at specific temperature steps are shown in Fig. 7. It can be noticed that in general, there is a broadening of peaks with increase in temperature as expected and a change in the relative intensity of the peaks. The distinctive Raman spectra of the Q phase similar to the ambient Raman spectrum were seen in the temperature range of $298 - 400\text{ K}$. However, with further increase in temperature, there are gradual changes observed in the spectra between 400 and 500 K . While four Raman modes could be seen ranging from 130 to 340 cm^{-1} until 400 K , we were able to fit only three peaks above 400 K . From this temperature the fitting procedure indicates, that the two modes around 248 and 275 cm^{-1} merge together and a new mode is seen at 260 cm^{-1} , which is accompanied by an abrupt change in the position and intensity of the other modes in the phonon bands (ν_5 and ν_6). This new mode continues to exist till higher temperatures. Also, the ν_3 mode at 671 cm^{-1} gradually decreases in intensity and disappears into the background after 400 K .

In order to clearly understand the variation in the spectra with the change of temperature, the peak positions of some of the intense Raman modes have been plotted with the increasing temperature, as shown in Fig. 8. Up to 400 K , all the phonon modes of NbO_6 octahedra show softening with increase in temperature, as expected. From 400 K , because of the rearrangement of modes, the two peaks around 210 and 260 cm^{-1} start to harden while the modes at 170 and 620 cm^{-1} [Nb-O symmetric stretching (ν_1) mode] continue to soften with small slope changes [48]. On further heating, all the internal vibrational modes of the octahedra show another anomaly and start softening above 500 K except the 170 cm^{-1} mode which does not undergo any significant changes. It is important to note that, as opposed to the expected behaviour, the 73 cm^{-1} peak assigned as the translational mode of Na^+ cation shows hardening in the entire temperature range while the librational mode at 110 cm^{-1} softens. We could also observe that most of the Raman modes show minor slope changes around 650 and 780 K .

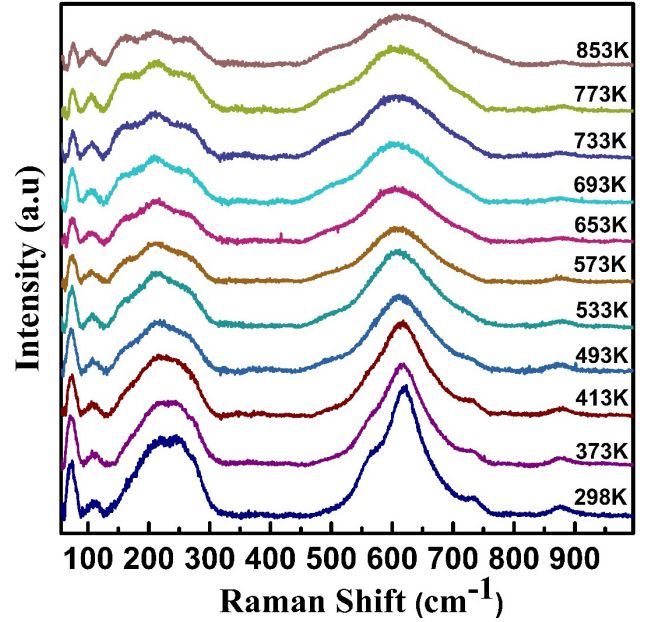


FIG. 7. The temperature-dependent evolution of Raman spectra at specific temperature steps.

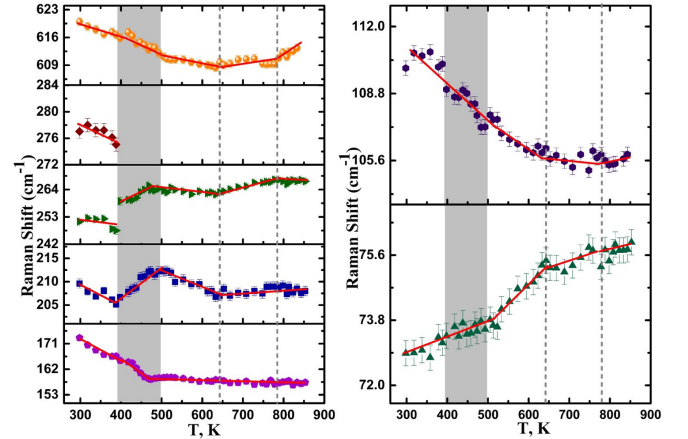


FIG. 8. Raman peak shift vs. temperature plots for different Raman modes during heating. The grey coloured region indicates the region of phase transition, while the dashed lines show possible additional anomalies. The solid red lines are guide to the eye.

IV. DISCUSSION

The $P(E)$ hysteresis loop measurements as well as the form of the $\varepsilon(E)$ curves reveal that sodium niobate in the NNO/SRO/(001)MgO heterostructure is in polar and switchable state and the electric polarization component exists along the normal to the substrate. However, the true direction of polarization can not be unambiguously determined from electric measurements because of the parallel geometry of electrodes, which can not exclude possible in-plane component of polarization.

It is reasonable to look for the candidates for the phases of NaNbO_3 observed at room and elevated temperatures in this work among those found in the bulk form of NNO or the phases related to them. The influence of epitaxial strain in $(001)\text{NaNbO}_3$ films has been studied using the DFT method in the recent work by Patel *et al.* [43]. Their results indicate that at compressive strains and tensile strains up to $\approx 1.27\%$ the monoclinically distorted N phase having the Cc symmetry is stabilized. In the narrow range of tensile strains between $\approx 1.27\%$ and $\approx 1.5\%$ the phase with $Pca2_1$ symmetry is found, which originates from the P bulk phase ($Pbcm$) by additional emergence of electric polarization along the $[001]$ orthorhombic direction. At tensile strains above $\approx 1.5\%$ the Q phase is found to possess the lowest energy.

Out of these three possible polar structures, namely the Cc , $Pca2_1$, and Q phases, the first two can be excluded from considerations because they contradict our x-ray observations. The Cc phase, similar to the bulk N phase, is characterized by distortions in the R-point of the PCBZ, but contrary to our results does not experience M-point distortions [25]. The $Pca2_1$ phase should show reflections in the Δ $(0, 0, 1/4)$ point of the PCBZ, which we do not observe in our experimental data. Therefore, among the obvious candidates only the Q phase remains potentially possible.

The Q phase appears due to the combination of the R, M, and Γ -point instabilities [24], which corresponds to our observations in reciprocal space imaging. Figure 4(a) shows schematical view of the unit cell of the Q phase and its relation to the pseudocubic unit cell, whereas Fig. 4(b) shows the corresponding view of the atomic positions and NbO_6 octahedra with indicated rotations due to the modes in the R and M points. Each domain of the bulk Q phase is characterized by a single M-point reflection, i.e., by either of M_H , M_K , or M_L point. In Fig. 4(a) the M_L point is active if we assume that the normal to the substrate is parallel to the vertical direction in the figure. At room temperature we observe reflections in the M_H and M_K points, which should stem from differently oriented domains of the studied structure. Considering the orthorhombic unit cell of the Q phase, one can note that there can be two different epitaxial contacts between the NaNbO_3 film and the $(001)\text{SrRuO}_3/\text{MgO}$ substrate. These two different epitaxial contacts are denoted by pink and yellow shaded faces as shown in Fig. 4(a), that should be constrained to the underlying SrRuO_3 layer. The respective top views of the structures are shown in Figs. 4(c) and (d). One should note here, that in the theoretical work of Patel *et al.* [43] only the "yellow"-type epitaxial contact has been considered, whereas the "pink" one has been overlooked.

Having identified the Q phase with "pink" epitaxial contact as the room temperature structure, we now come to the question on how this structure changes upon heating and what is the origin of the broad peak in the dielectric constant. Upon increasing temperature, the diffraction pattern gradually changes due to appearance of re-

flections in the M_L -type points and extinction of the M_H and M_K points. The structure with M_L -type reflections corresponds then to the "yellow"-type epitaxial contact with electric polarization parallel to the substrate, as shown in Fig. 4(d). However, the presence or absence of electric polarization in the high-temperature phase can not be judged upon based on the available experimental data, because our x-ray diffraction results are consistent with the "yellow" Q phase epitaxy, but can not confirm the presence of polar distortions. In principle the high-temperature structure can be characterized only by R and M point distortions, which may correspond to the bulk T_1 phase [25]. However, the possibility of the T_1 phase option seems to us less likely since this phase appears in the bulk at substantially higher temperatures.

The variant with temperature-driven change of Q phase epitaxy between the "pink" and "yellow" orientations is interesting because it presents a rare type of phase transitions in films, which was extensively discussed in theoretical works earlier, and at the same time can explain the observed broad maximum of the dielectric constant. Such a phase transition between two orthorhombic phases with differently oriented polarizations has not been studied according to our knowledge. However, a phase transition in PbTiO_3 films between two tetragonal phases a and c with in-plane and out-of-plane orientations of polarization, respectively, has been studied theoretically by Pertsev *et al.* [42]. The results indicate that the dielectric constant experiences a maximum across this phase transition. Thus, one may expect similar behavior across the phase transition between two orthorhombic phases observed in our case.

The results from the dielectric measurements and the reciprocal space mapping are further corroborated by the Raman spectroscopy data, which suggest the presence of Q phase structure at room temperature. The Raman spectroscopy data reveal changes in the Raman spectra at 400 and 500 K, which, thus, supports the results of the other measurement methods showing a broad and diffuse phase transition in this temperature range. The anomalies in the Raman spectra at 400 and 500 K consist in the disappearance of certain modes upon heating and slope changes in the peak positions of modes when plotted against temperature. This disappearance of modes is consistent with the change of Q phase orientation from "pink" to "yellow". As our sample is a highly oriented thin film, any change in the orientation of the orthorhombic Q phase cell should be reflected in the Raman spectra taken in the same backscattering geometry. The reduced number of modes observed above 400 K is in qualitative correspondence with the change in epitaxial contacts of the Q phase because of the Raman scattering selection rules for the two considered orientations. Indeed, in the case of the "pink"-type epitaxial contact, the employed backscattering geometry of the experiment allows the modes $A_1(\text{LO})$, $A_1(\text{TO})$, A_2 , and $B_1(\text{TO})$, whereas the "yellow"-type contact allows only the $A_1(\text{TO})$ and $B_2(\text{TO})$ modes [54, 55].

In contrast to x-ray and dielectric measurements, the changes observed in the Raman spectroscopy are more abrupt. However, one has to keep in mind the different scales at which the information is gathered in these methods. In the case of Raman measurements the dimensions of the laser spot is of the order of several microns and the spectra are averaged over a low number of different domains, whereas in the case of x-ray and dielectric methods the dimensions are of the order of hundreds of microns, which results in averaging over many different domains. Furthermore, although we also observe some slope changes in Raman spectra on further heating around 650 and 780 K, the exact nature of these anomalies could not be proposed from the Raman data alone. They might still reflect the gradual changes observed in reciprocal space mapping up to the highest measured temperature (773 K), since the anomalies in the Raman spectra fall into the temperature range covered by the x-ray diffraction.

V. CONCLUSIONS

Using the combination of the dielectric, x-ray diffraction, and Raman spectroscopy measurement methods we showed that NaNbO_3 film in the synthesized $\text{NaNbO}_3/\text{SrRuO}_3/(001)\text{MgO}$ heterostructure experiences a diffuse phase transition above room tempera-

ture. Our results allow concluding that this transition is related to the transition between two different orientations of the Q phase, that have different epitaxial conjugations with the underlying $\text{SrRuO}_3/(001)\text{MgO}$ structure. This phenomenon is remarkably interesting because such phase transitions have attracted attention earlier in theoretical works [40–42, 44], however their experimental characterization is limited. The discovered behavior of NNO films can be potentially interesting for the development of applications in memory, logic, sensing, and energy harvesting devices.

ACKNOWLEDGMENTS

C.N., A.J., and J.S performed Raman studies and acknowledge JNCASR/TRC for the Raman Spectrometer facility. A.J. and J.S. acknowledge Jawaharlal Nehru Centre for Advanced Scientific Research for providing research fellowships (JNC/S0752 and JNC/S0539), which supported Raman measurements and data treatment. M.V.V., A.E.G., S.A.U., and R.G.B. performed x-ray diffraction studies. A.V.P., D.V.S., I.P.R., and N.V.T. have conceptualized the study, performed synthesis, dielectric measurements, and collaborative interpretation of results under the financial support by the Russian Science Foundation grant No. 19-12-00205.

-
- [1] H. D. Megaw, The seven phases of sodium niobate, *Ferroelectrics* **7**, 87 (1974).
 - [2] M. E. Lines and A. M. Glass, *Principles and Applications of Ferroelectrics and Related Materials* (Clarendon Press, Oxford, 1977).
 - [3] H. Palneedi, M. Peddigari, G. Hwang, D. Jeong, and J. Ryu, High-performance dielectric ceramic films for energy storage capacitors: Progress and outlook, *Adv. Funct. Mater.* **28**, 1803665 (2018).
 - [4] J. Wu, D. Xiao, and J. Zhu, Potassium–sodium niobate lead-free piezoelectric materials: Past, present, and future of phase boundaries, *Chem. Rev.* **115**, 2559 (2015).
 - [5] A. Chauhan, S. Patel, R. Vaish, and C. Bowen, Antiferroelectric ceramics for high energy density capacitors, *Materials* **8**, 8009–8031 (2015).
 - [6] R. Zuo, H. Qi, J. Fu, J. Li, M. Shi, and Y. Xu, Giant electrostrictive effects of $\text{NaNbO}_3\text{-BaTiO}_3$ lead-free relaxor ferroelectrics, *Appl. Phys. Lett.* **108**, 232904 (2016).
 - [7] M. Zhou, R. Liang, Z. Zhou, and X. Dong, Potentiality of Bi and Mn co-doped lead-free NaNbO_3 ceramics as a pyroelectric material for uncooled infrared thermal detectors, *J. Eur. Ceram. Soc.* **39**, 2058 (2019).
 - [8] L. Zhang, C. Zhao, T. Zheng, and J. Wu, Large electrocaloric response with superior temperature stability in NaNbO_3 -based relaxor ferroelectrics benefiting from the crossover region, *J. Mater. Chem. A* **9**, 2806 (2021).
 - [9] S. K. Mishra, N. Choudhury, S. L. Chaplot, P. S. R. Krishna, and R. Mittal, Competing antiferroelectric and ferroelectric interactions in NaNbO_3 : Neutron diffraction and theoretical studies, *Phys. Rev. B* **76**, 024110 (2007).
 - [10] M. D. Peel, S. P. Thompson, A. Daoud-Aladine, S. E. Ashbrook, and P. Lightfoot, New twists on the perovskite theme: Crystal structures of the elusive phases R and S of NaNbO_3 , *Inorganic Chemistry* **51**, 6876 (2012).
 - [11] C. N. W. Darlington and K. S. Knight, On the lattice parameters of sodium niobate at room temperature and above, *Physica B: Condensed Matter* **266**, 368 (1999).
 - [12] S. I. Raevskaya, I. P. Raevski, S. P. Kubrin, M. S. Panchelyuga, V. G. Smotrakov, V. V. Eremkin, and S. A. Prosandeev, Quantum paraelectricity coexisting with a ferroelectric metastable state in single crystals of NaNbO_3 : a new quantum effect, *J. Phys.: Condens. Matter* **20**, 232202 (2008).
 - [13] L. Jiang, D. C. Mitchell, W. Dmowski, and T. Egami, Local structure of NaNbO_3 : A neutron scattering study, *Phys. Rev. B* **88**, 014105 (2013).
 - [14] I. Lefkowitz, K. Łukaszewicz, and H. D. Megaw, The high-temperature phases of sodium niobate and the nature of transitions in pseudosymmetric structures, *Acta Cryst.* **20**, 670 (1966).
 - [15] J. Chen and D. Feng, TEM study of phases and domains in NaNbO_3 at room temperature, *Phys. Stat. Sol. A* **109**, 171 (1988).
 - [16] J. Chen and D. Feng, In situ TEM studies of para-ferro phase transitions in NaNbO_3 , *Phys. Stat. Sol. A* **109**, 427 (1988).
 - [17] R. A. Shakhovoy, S. I. Raevskaya, L. A. Shakhovaya, D. V. Suzdalev, I. P. Raevski, Y. I. Yuzyuk, A. F. Se-

- menchev, and M. El Marssi, Ferroelectric Q and antiferroelectric P phases' coexistence and local phase transitions in oxygen-deficient NaNbO_3 single crystal: micro-Raman, dielectric and dilatometric studies, *J. Raman Spectrosc.* **43**, 1141 (2012).
- [18] Y. Shiratori, A. Magrez, J. Dornseiffer, F. Haegel, C. Pithan, and R. Waser, Polymorphism in micro-, submicro-, and nanocrystalline NaNbO_3 , *J. Phys. Chem. B* **109**, 20122 (2005).
- [19] J. Koruza, J. Tellier, B. Malič, V. Bobnar, and M. Kosec, Phase transitions of sodium niobate powder and ceramics, prepared by solid state synthesis, *J. Appl. Phys.* **108**, 113509 (2010).
- [20] J. Koruza, P. Groszewicz, H. Breitzke, G. Buntkowsky, T. Rojac, and B. Malič, Grain-size-induced ferroelectricity in NaNbO_3 , *Acta Mater.* **126**, 77 (2017).
- [21] L. E. Cross and B. J. Nicholson, The optical and electrical properties of single crystals of sodium niobate, *Philos. Mag.* **46**, 453 (1955).
- [22] L. E. Cross, Electric double hysteresis in $(\text{K}_x\text{Na}_{1-x})\text{NbO}_3$ single crystals, *Nature* **181**, 178 (1958).
- [23] A. V. Ulinzheyev, O. E. Fesenko, and V. G. Smotrakov, Super-high field-induced phase transitions in NaNbO_3 crystals, *Ferroelectrics Lett.* **12**, 17 (1990).
- [24] W. Cochran and A. Zia, Structure and dynamics of perovskite-like crystals, *Phys. Stat. Sol.* **25**, 273 (1968).
- [25] P. Tolédano and D. D. Khalyavin, Symmetry-determined antiferroelectricity in PbZrO_3 , NaNbO_3 , and PbHfO_3 , *Phys. Rev. B* **99**, 024105 (2019).
- [26] N. Setter, D. Damjanovic, L. Eng, G. Fox, S. Gevorgian, S. Hong, A. Kingon, H. Kohlstedt, N. Y. Park, G. B. Stephenson, I. Stolitchnov, A. K. Taganstev, D. V. Taylor, T. Yamada, and S. Streiffer, Ferroelectric thin films: Review of materials, properties, and applications, *J. Appl. Phys.* **100**, 051606 (2006).
- [27] D. Sando, Y. Yang, C. Paillard, B. Dkhil, L. Bellaiche, and V. Nagarajan, Epitaxial ferroelectric oxide thin films for optical applications, *Appl. Phys. Rev.* **5**, 041108 (2018).
- [28] S. R. Burns and M. R. Dolgos, Sizing up $(\text{K}_{1-x}\text{Na}_x)\text{NbO}_3$ films: a review of synthesis routes, properties & applications, *New J. Chem.* **45**, 7408 (2021).
- [29] Y. I. Yuzyuk, R. A. Shakhovoy, S. I. Raevskaya, I. P. Raevskii, M. El Marssi, M. G. Karkut, and P. Simon, Ferroelectric Q-phase in a NaNbO_3 epitaxial thin film, *Appl. Phys. Lett.* **96**, 222904 (2010).
- [30] S. Yamazoe, A. Kohori, H. Sakurai, Y. Kitanaka, Y. Noguchi, M. Miyayama, and T. Wada, Laser beam scanning microscope and piezoresponse force microscope studies on domain structured in 001-, 110-, and 111-oriented NaNbO_3 films, *J. Appl. Phys.* **112**, 052007 (2012).
- [31] S. Oda, T. Saito, H. Adachi, and T. Wada, Preparation of ferroelectric NaNbO_3 thin films on MgO substrate by pulsed laser deposition, *IEEE Trans. Ultrason. Ferroelectr. Freq. Control* **55**, 1017 (2008).
- [32] S. Yamazoe, H. Sakurai, M. Fukada, H. Adachi, and T. Wada, The effect of SrTiO_3 substrate orientation on the surface morphology and ferroelectric properties of pulsed laser deposited NaNbO_3 films, *Appl. Phys. Lett.* **95**, 062906 (2009).
- [33] M. Tyunina and J. Levoska, Unstable state in epitaxial films of sodium niobate, *Appl. Phys. Lett.* **95**, 102903 (2009).
- [34] B. Cai, J. Schwarzkopf, E. Hollmann, M. Schmidbauer, M. O. Abdel-Hamed, and R. Wördenweber, Anisotropic ferroelectric properties of anisotropically strained epitaxial NaNbO_3 films, *J. Appl. Phys.* **115**, 224103 (2014).
- [35] A. Duk, M. Schmidbauer, and J. Schwarzkopf, Anisotropic one-dimensional domain pattern in NaNbO_3 epitaxial thin films grown on (110) TbScO_3 , *Appl. Phys. Lett.* **102**, 091903 (2013).
- [36] J. Schwarzkopf, D. Braun, M. Schmidbauer, A. Duk, and R. Wördenweber, Ferroelectric domain structure of anisotropically strained NaNbO_3 epitaxial thin films, *J. Appl. Phys.* **115**, 204105 (2014).
- [37] T. Mino, S. Kuwajima, T. Suzuki, I. Kanno, H. Kotera, and K. Wasa, Piezoelectric properties of epitaxial NaNbO_3 thin films deposited on (001) $\text{SrRuO}_3/\text{Pt}/\text{MgO}$ substrates, *Jpn. J. Appl. Phys.* **46**, 6960 (2007).
- [38] A. V. Pavlenko, D. V. Stryukov, and N. V. Ter-Oganessian, Structure and ferroelectric properties of thin heteroepitaxial NaNbO_3 films obtained by RF cathode sputtering, *Techn. Phys. Lett.* **46**, 62 (2020).
- [39] O. Diéguez, K. M. Rabe, and D. Vanderbilt, First-principles study of epitaxial strain in perovskites, *Phys. Rev. B* **72**, 144101 (2005).
- [40] N. A. Pertsev, A. G. Zembilgotov, and A. K. Tagantsev, Effect of mechanical boundary conditions on phase diagrams of epitaxial ferroelectric thin films, *Phys. Rev. Lett.* **80**, 1988 (1998).
- [41] N. A. Pertsev, A. G. Zembilgotov, and A. K. Tagantsev, Equilibrium states and phase transitions in epitaxial ferroelectric thin films, *Ferroelectrics* **223**, 79 (1999).
- [42] N. A. Pertsev, V. G. Koukhar, R. Waser, and S. Hoffmann, Effects of domain formation on the dielectric properties of ferroelectric thin films, *Integr. Ferroelectrics* **32**, 235 (2001).
- [43] K. Patel, S. Prosandeev, B. Xu, C. Xu, and L. Bellaiche, Properties of (001) NaNbO_3 films under epitaxial strain: A first-principles study, *Phys. Rev. B* **103**, 094103 (2021).
- [44] N. A. Pertsev, V. G. Kukhar, H. Kohlstedt, and R. Waser, Phase diagrams and physical properties of single-domain epitaxial $\text{Pb}(\text{Zr}_{1-x}\text{Ti}_x)\text{O}_3$ thin films, *Phys. Rev. B* **67**, 054107 (2003).
- [45] E. Husson and Y. Repelin, Etude par spectroscopie vibrationnelle des niobates de sodium et d'argent de structure perovskite, *Spectrochimica Acta A* **40**, 315 (1984).
- [46] Y. D. Juang, M. L. Hu, and W. S. Tse, Temperature-dependent Raman-scattering studies of $\text{Li}_{0.02}\text{Na}_{0.98}\text{NbO}_3$, *J. Appl. Phys.* **76**, 3746 (1994).
- [47] X. Wang, Z. Shen, Z. Hu, L. Qin, S. Tang, and M. Kuok, High temperature Raman study of phase transitions in antiferroelectric NaNbO_3 , *J. Mol. Struct.* **385**, 1 (1996).
- [48] Z. X. Shen, X. B. Wang, M. H. Kuok, and S. H. Tang, Raman scattering investigations of the antiferroelectric-ferroelectric phase transition of NaNbO_3 , *J. Raman Spectr.* **29**, 379 (1998).
- [49] E. Bouziane, M. D. Fontana, and M. Ayadi, Study of the low-frequency Raman scattering in NaNbO_3 crystal, *J. Phys.: Condens. Matter* **15**, 1387 (2003).
- [50] R. Jiménez, M. L. Sanjuán, and B. Jiménez, Stabilization of the ferroelectric phase and relaxor-like behaviour in low Li content sodium niobates, *J. Phys.: Condens. Matter* **16**, 7493 (2004).
- [51] Y. I. Yuzyuk, P. Simon, E. Gagarina, L. Hennet, D. Thi-audière, V. I. Torgashev, S. I. Raevskaya, I. P. Raevskii,

- L. A. Reznitchenko, and J. L. Sauvajol, Modulated phases in NaNbO_3 : Raman scattering, synchrotron x-ray diffraction, and dielectric investigations, *J. Phys.: Condens. Matter* **17**, 4977 (2005).
- [52] S. J. Lin, D. P. Chiang, Y. F. Chen, C. H. Peng, H. T. Liu, J. K. Mei, W. S. Tse, T.-R. Tsai, and H.-P. Chiang, Raman scattering investigations of the low-temperature phase transition of NaNbO_3 , *J. Raman Spectr.* **37**, 1442 (2006).
- [53] S. D. Ross, The vibrational spectra of lithium niobate, barium sodium niobate and barium sodium tantalate, *J. Phys. C* **3**, 1785 (1970).
- [54] M. I. Aroyo, J. M. Perez-Mato, C. Capillas, E. Kroumova, S. Ivantchev, G. Madariaga, A. Kirov, and H. Wondratschek, Bilbao crystallographic server: I. Databases and crystallographic computing programs, *Z. Krist.* **221**, 15 (2006).
- [55] M. I. Aroyo, A. Kirov, C. Capillas, J. M. Perez-Mato, and H. Wondratschek, Bilbao crystallographic server. II. Representations of crystallographic point groups and space groups, *Acta Cryst. A* **62**, 115 (2006).